Multiparticle production in p-p, p-Ar, and p-Xe collisions at 200 GeV by the multistring model VENUS

K. Werner
Physics Department, Brookhaven National Laboratory, Upton, New York 11973
(Received 28 June 1988)

We give a detailed description of the multistring model VENUS for nucleon-nucleus collisions at ultrarelativistic energies. According to the model, color strings are formed as a consequence of color exchange between quarks of colliding nucleons. Sequences of nucleon-nucleon collisions are determined from geometrical considerations. We calculate, among other things, multiplicity distribution for various rapidity intervals for p-p, p-Ar, and p-Xe at 200 GeV, to compare with negative-binomial fits to data.

I. INTRODUCTION

The ultimate goal of the heavy-ion experiments at Brookhaven and CERN is to find a new kind of matter: the quark-gluon plasma (QGP) (Refs. 1 and 2). The asymptotic-freedom property of QCD implies that at high temperatures and/or densities such a gas of free quarks and gluons should exist, the temperature being low enough to be reached in current heavy-ion experiments. The occurrence of such a new phenomenon should be proven by an unexpected behavior of one or more observables, which requires, of course, the knowledge of "expected behavior." Unfortunately, nobody can calculate what to expect in an ultrarelativistic nucleus-nucleus collision, even without a QGP state involved—we have to rely on models.

One class of model can be considered as an extrapolation of proton-proton (p-p) scattering. The philosophy is (1) to construct (and test) a parton model for p-p scattering and (2) determine, from nuclear geometry, p-p interactions in a nucleus-nucleus collision and treat then every p-p interaction in the same way as an isolated p-p collision. This amounts not as a superposition of p-p collisions, since a nucleon after an interaction is most probably a dressed diquark (or even quark) rather than a proton. Several models have been constructed along these lines: LUND models[3,4] assume that every p-p collision results in excited baryons. A phenomenological excitation function determines excitation energy and momentum of the baryon, which is further on treated as a particle-producing string. Another class of models are motivated by Regge phenomenology, such as dual parton models[5–7] and VENUS (Ref. 8), which will be described in this paper. Here the basic mechanism to form strings is color exchange between the quarks of colliding nucleons. An advantage over LUND is that string properties can be calculated from structure functions (though an extrapolation toward low-momentum transfer is necessary). For a comparison of the models see Ref. 9.

In order to test such extrapolation models, proton-nucleus collisions should be considered very useful, since certain aspects of the reaction mechanism are much cleaner in pA than in A-A collisions. For example, considering p-p, p-Ar, and p-Xe collisions (with average number of collisions $\langle\nu\rangle_{\mathrm{Ar}}\approx 2$ and $\langle\nu\rangle_{\mathrm{Xe}}\approx 3$) we can compare a proton colliding once, twice, and three times with target nucleons. The average collision numbers are obtained from

$$\langle\nu\rangle_A=\sum_{\nu\geq 1}\nu P_A(\nu)\ ,$$

$P_A(\nu)$ being the probability for an incident proton to perform ν collisions inside the nucleus A. Distributing the nucleons randomly according to the nuclear density $\rho_A(\mathbf{x})$ we obtain an average number of collisions for a given impact parameter b of

$$\langle\nu\rangle_b=\sigma_{\mathrm{in}}\int dz\,\rho_A(b,z) \tag{1.1}$$

leading to an impact-parameter average over Poisson distributions[10] for $P_A(\nu)$:

$$P_A(\nu)=\int d^2b\frac{(\langle\nu\rangle_b)^\nu}{\nu!}e^{-\langle\nu\rangle_b}\ . \tag{1.2}$$

Since the cross section can be expanded as

$$\sigma_{pA}=\sum_{\nu\geq 1}P_A(\nu)\sigma_\nu\ , \tag{1.3}$$

we can also study even more than three collisions in a p-Xe scattering. However, as can be seen from Eq. (1.2), $P_A(\nu)$ is for ν larger than $\langle\nu\rangle_{b=0}$ a very fast-decreasing function of ν (see Fig. 1), so it might be difficult to see large-ν effects.

II. MULTIPLE SCATTERING

The basic assumption of our model is that the projectile nucleon—whatever its nature is after the first collision—moves through the nucleus on a straight line, interacting with nucleons coming into its way. Each interaction means color exchange and string formation; we will discuss that in detail later. The projectile is assumed to be outside the nucleus already when it hadronizes.

This is reasonable as long as the hadronization time

$$\tau_h=m^{-1}\cosh(y)$$

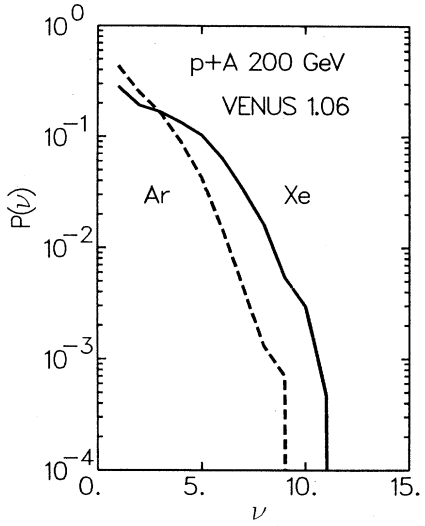

FIG. 1. The distribution $P(\nu)$ of the number of collision ν for p-Ar and p-Xe collisions. Mean values are $\langle\nu\rangle_{\mathrm{Ar}}=2.13$ and $\langle\nu\rangle_{\mathrm{Xe}}=3.04$.

for the leading particle is much larger than the reaction time

$$\tau_r = 2R\ \coth(y)\ , \tag{2.1}$$

R being the nuclear radius. A condition for the applicability of our model is, therefore,

$$\tau_h > \tau_r\ . \tag{2.2}$$

For 200-GeV incident energy with $y=6$ we obtain $\tau_h \approx 40$ fm/c and $\tau_r \approx 2R$, so the condition $\tau_h > \tau_r$ is satisfied for all nuclei. At 14.5 GeV with $y=3.4$ we find $\tau_h \approx 3$ fm/c, which means the projectile hadronizes inside the nucleus—the model should not work. If (2.2) is violated, it may be useful to introduce another time scale, the time τ_c between two nucleon-nucleon interactions

$$\tau_c = \lambda \coth(y)\ , \tag{2.3}$$

with λ being the nuclear mean-free path. For 14.5 GeV we get $\tau_c \approx 2$ fm/c, so the projectile can perform two collisions before it hadronizes—we need a kind of hybrid model.

Let us consider a proton with high enough energy (so that the condition $\tau_h > \tau_r$ is satisfied) hitting a nucleus with mass number A. Our reference system is the center-of-mass system of the incident nucleon and one target nucleon, further on referred to as the N-N c.m. system, having the rapidity

$$\begin{aligned} y_{\mathrm{c.m.}} &= \tfrac{1}{2}\times\tfrac{1}{2}\ln\frac{E+P}{E-P} \\ &= \tfrac{1}{2}\ln\frac{(m^2+P^2)^{1/2}+P}{m} \\ &\approx \tfrac{1}{2}\ln\frac{2P}{m}\ . \end{aligned} \tag{2.4}$$

The NN energy in this system is

$$\begin{aligned} \sqrt{s_{NN}} &= \{[(m^2+P^2)^{1/2}+m]^2-P^2\}^{1/2} \\ &\approx \sqrt{2Pm}\ , \end{aligned} \tag{2.5}$$

the last equalities being true in the ultrarelativistic limit $P \gg m$ (m is the nucleon mass). In the numerical calculations we always use the exact formulas. For 200-GeV incident nucleons, for example, we obtain from (2.4) and (2.5) $y_{\mathrm{c.m.}}=3.0$ and $\sqrt{s_{NN}}=19.4$, for 14.5 GeV we find $y_{\mathrm{c.m.}}=1.7$ and $\sqrt{s_{NN}}=5.4$. From (2.5) we obtain the initial momenta for the projectile nucleon

$$E_0 = \frac{\sqrt{s_{NN}}}{2} \approx \left[\frac{Pm}{2}\right]^{1/2}\ , \tag{2.6}$$

$$P_0^{\parallel} = (E_0^2-m^2)^{1/2} \tag{2.7}$$

and the target nucleons

$$E_i = \frac{\sqrt{s_{NN}}}{2} \approx \left[\frac{Pm}{2}\right]^{1/2}\ ,\quad i=1,A \tag{2.8}$$

$$P_i^{\parallel} = -(E_i^2-m^2)^{1/2},\quad i=1,A\ . \tag{2.9}$$

Correspondingly, the coordinates of the nucleons are labeled as (x_0,y_0,z_0) and (x_i,y_i,z_i), $i=1,A$. The target nucleons are distributed isomorphically according to a Woods-Saxon density distribution

$$\rho(r) = \frac{\rho_0}{1+\exp[(r-r_0)/a]} \tag{2.10}$$

with the parameters

$$a=0.54,\quad r_0 = 1.19A^{1/3}-1.61A^{-1/3}\ . \tag{2.11}$$

Although not very important, we take into account the hard core of the nucleon:

$$(x_i-x_j)^2+(y_i-y_j)^2+(z_i-z_j)^2 \geq (2r_c)^2 \tag{2.12}$$

with a core radius $r_c=0.4$ fm. The projectile nucleon N_0 is assumed to move on a straight line through the nucleus, making an interaction whenever it comes close enough to a target nucleon N_i:

$$(x_0-x_i)^2+(y_0-y_i)^2 \leq \frac{\sigma_{NN}}{\pi}\ , \tag{2.13}$$

σ_{NN} being the inelastic N-N cross section (we use $\sigma_{NN}=3.1$ fm^2 for 200 GeV). As discussed later, a nucleon is usually no longer a nucleon after it hits a target nucleon. Nevertheless, we believe this "object" to travel through the nucleus still having the size of a nucleon and having the same mean-free path; therefore we use the same σ_{NN} independent of how many collisions are performed.

Before we discuss in the next section what we mean by nucleon-nucleon interaction (color exchange, string formation, . . .), we want to investigate how many interactions we expect according to the above scenario. In Fig. 1 we display Monte Carlo results (using VENUS 1.06) for the probability $P(\nu)$ for an incident proton to hit [according to Eq. (2.13)] ν target nucleons for an argon and

a xenon target. For the mean-collision numbers $\langle\nu\rangle=\sum\nu P(\nu)$ we obtain 2.12 for argon and 3.04 for xenon. We notice that $P(\nu)$ is a rapidly decreasing function of ν with a maximum at $\nu=1$ (which remains also true for heavy targets). This means that nucleon-nucleus collisions are dominated by peripheral collisions with a single nucleon-nucleon interaction, which is rather unfortunate, since we do not want to study p-p collisions in p-A experiments. The hard-core radius r_c [see Eq. (2.12)] only weakly affects the distribution $P(\nu)$, so we are going to provide some explicit formulas for $r_c=0$. Since the computer code is flexible enough to allow a change of the elementary cross section σ_{NN} with the number of collisions (although this is never done in numerical calculations), let us consider a sequence σ_i $(1\le i\le\nu+1)$ of elementary cross sections for the ith collision, implying mean free paths $[\sigma_i\rho(\mathbf{x})]^{-1}$. The probability to perform a collision between z and $z+dz$ is

$$\sigma_i\rho(b,z)dz\ ; \tag{2.14}$$

the probability for no collision is

$$1-\sigma_i\rho(b,z)dz=\exp[-\sigma_i\rho(b,z)dz]\ ; \tag{2.15}$$

so the probability for ν collisions between z_i and z_i+dz_i $(1\le i\le\nu)$ is

$$\begin{aligned}dP_\nu(b)=&\exp\left[-\int_{-\infty}^{z_1}\sigma_1\rho(b,z)dz\right]\sigma_1\rho(b,z_1)dz_1\\&\times\exp\left[-\int_{z_1}^{z_2}\sigma_2\rho(b,z)dz\right]\sigma_2\rho(b,z_2)dz_2\\&\times\cdots\\&\times\exp\left[-\int_{z_\nu}^{\infty}\sigma_{\nu+1}\rho(b,z)dz\right]\ .\end{aligned}\tag{2.16}$$

Introducing

$$\tau_i:\equiv\int_{-\infty}^{z_i}\rho(b,z)dz \tag{2.17}$$

and

$$T:\equiv\int_{-\infty}^{\infty}\rho(b,z)dz \tag{2.18}$$

we obtain, by using $d\tau_i=\rho(b,z_i)dz_i$,

$$\begin{aligned}dP_\nu(b)=&\exp(-\sigma_1\tau_1)\sigma_1 d\tau_1\\&\times\exp[-\sigma_2(\tau_2-\tau_1)]\sigma_2 d\tau_2\\&\times\cdots\\&\times\exp[-\sigma_{\nu+1}(T-\tau_\nu)]\ .\end{aligned}\tag{2.19}$$

Integrating Eq. (2.19) we obtain for the probability to perform ν collisions (at a given impact parameter)

$$P_\nu(b)=\left[\prod_{i=1}^{\nu}\sigma_i\right]\exp[-\sigma_{\nu+1}T(b)]\int_0^{T(b)}\cdots\int_0^{T(b)}d\tau_1\cdots d\tau_\nu\left[\prod_{i=1}^{\nu}\theta(\tau_{i+1}-\tau_i)\right]\exp\left[-\sum_{i=1}^{\nu}(\sigma_i-\sigma_{i+1})\tau_i\right]\ . \tag{2.20}$$

Equation (2.20) simplifies considerably for equal elementary cross sections $\sigma_i=\sigma$ (this is used in all calculations shown in this paper). In this case we have $\sigma_i-\sigma_{i+1}=0$, and we get, from (2.20),

$$P_\nu(b)=\sigma^\nu\exp[-\sigma T(b)]\int_0^{T(b)}\cdots\int_0^{T(b)}d\tau_1\cdots d\tau_\nu\left[\prod_{i=1}^{\nu}\theta(\tau_{i+1}-\tau_i)\right]\ . \tag{2.21}$$

The integration yields $T(b)^\nu/\nu!$, so we get with $\langle\nu\rangle_b\equiv\sigma T(b)$ a Poissian distribution

$$P_\nu(b)=\frac{(\langle\nu\rangle_b)^\nu}{\nu!}\exp(-\langle\nu\rangle_b)\ . \tag{2.22}$$

This is Glauber's result already quoted earlier [see Eq. (1.2)]. Numerical integration of

$$P_\nu=2\pi\int db\ b\frac{(\langle\nu\rangle_b)^\nu}{\nu!}\exp(-\langle\nu\rangle_b) \tag{2.23}$$

gives results very close to the curves shown in Fig. 1, which are derived with the Monte Carlo technique. From Eq. (2.23) it is obvious that $P(\nu)$ drops very fast whenever ν exceeds $\langle\nu\rangle_{b=0}$ ($\langle\nu\rangle_{b=0}$ is of the order $2R/\langle\lambda\rangle$, so $\langle\nu\rangle_{b=0}$ is approximately 5.4 for Xe and 3.6 for Ar).

III. STRING FORMATION

In this section we want to specify what we mean by nucleon-nucleon interaction. Let us first consider the interaction of two "fresh" nucleons, not having performed an interaction before (i.e., a pure N-N collision). The interaction between the two nucleons is realized by color exchange between a quark of the projectile and a quark of the target (see Ref. 5). Since particle production in ultrarelativistic collisions is very much forward peaked, thus limiting the transfer of transverse momentum, we assume that the color exchange occurs without any momentum transfer. The production of massive strings is just due to the fact that color exchange causes the formation of color singlets—stretched between partons from different nuclei. The relative motion of the partons creates the string mass.

We make the general ansatz, that the whole N-N collision is a superposition of contributions σ_i with i color exchanges

$$\sigma=\sum_i w_i\sigma_i\ , \tag{3.1}$$

w_i being the probability for such a contribution. We first describe the basic one-color-exchange contribution σ_1. As shown in Fig. 2(a), color exchange (arrow) between a projectile quark and a target quark rearranges the color structure such that instead of two nucleons in singlet states we find two singlets each consisting of a diquark and a quark of the other nucleon. We explicitly treat the case in which one (or both) of the quarks participating in

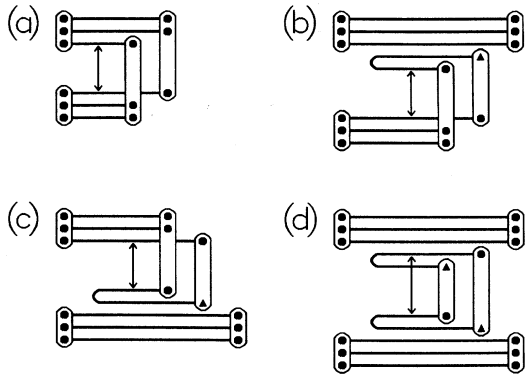

FIG. 2. The four basic one-color-exchange diagrams. The arrows indicate color exchange between quarks, leading to a rearrangement of singlets (string formation). The contributions (a)–(d) differ in the number N of white $q\bar{q}$ pairs involved: $N=0$ (a), $N=1$ (b) and (c), $N=2$ (d).

the color exchange is accompanied by an antiquark such that the $q\bar{q}$ pair is color neutral, because in this case the diquark-quark (qq-q) string is replaced by a q-$\bar{q}$ string and a baryon. In Figs. 2(b)–2(d) we show this for the case when the projectile quarks 2(b), the target quark 2(c), or both quarks 2(d) are part of colorless $q\bar{q}$ pairs. We generate quarks with and without $\bar{q}$ partners with probabilities w and $1-w$, so the relative weights of these contributions σ_1^a, σ_1^b, σ_1^c, σ_1^d can be expressed in terms of w

$$P(\sigma_1^a)=(1-w)^2, \quad P(\sigma_1^b)=w(1-w)\ , \\ P(\sigma_1^c)=w(1-w), \quad P(\sigma_1^d)=w^2\ . \tag{3.2}$$

In order to qualitatively understand the properties of the different diagrams concerning particle production, it is sufficient to know that the quarks (antiquarks) participating in the color exchange are most likely very slow—according to the quark structure functions. That means that all the q-$\bar{q}$ strings, consisting of a slow-forward-moving quark and a slow-backward-moving antiquark (or vice versa) have a much smaller mass than the qq-q strings, where a fast diquark participates. Whereas contribution 2(a) is of course symmetric in the N-N c.m. system, we expect for 2(b) a fast nucleon in forward direction, and a bunch of particles produced preferentially in backward direction from qq-q string fragmentation. This is the typical situation for diffractive target excitation due to Pomeron exchange. Another similarity concerns the momentum distribution of the scattered nucleon. Because of the x^{-1} divergence of sea-quark structure functions, the momentum fraction of the nucleon $x_N=1-x_q-x_{\bar{q}}$ is distributed as $(1-x_N)^{-1}$ as observed for diffractive scattering and as predicted due to Pomeron exchange (for details see Ref. 11). Since the mass of the qq-q string is roughly given as (neglecting parton masses and transverse momentum) $m^2=s_{NN}x$, with x being the quark momentum fraction, the x^{-1} divergence of the sea-quark structure functions also implies an m^{-2} behavior for missing-mass distributions—as observed in diffractive scattering. For all these reasons we refer to the contributions 2(a)–2(d) from the figure as 2(a) nondiffractive, 2(b) diffractive target excitation, 2(c) diffractive projectile excitation, and 2(d) double-Pomeron exchange.

Higher-order contributions—involving several color exchanges—are obtained by applying the basic contribution σ_1^a, σ_1^b, σ_1^c, σ_1^d [corresponding to Figs. 2(a)–2(d)] several times

$$\sigma_i=(\sigma_1)^i=\left[\sum_{m\in M}P(\sigma_1^m)\sigma_1^m\right]^i \\ =\sum_{m_1\in M}\cdots\sum_{m_i\in M}\prod_{j=1}^{i}P(\sigma_1^{m_j})\prod_{j=1}^{i}\sigma_1^{m_j} \tag{3.3}$$

with the set M defined as $M\equiv\{a,b,c,d\}$. In Fig. 3 we show three of the 16 possibilities for $i=2$ (two-color-exchange) contributions: $\sigma_1^d\sigma_1^d$, $\sigma_1^d\sigma_1^a$, and $\sigma_1^a\sigma_1^a$. From the point of view of the projectile (upper nucleon) in contribution (dd) the projectile survives, whereas in (da) the nucleon breaks up leaving a "leading diquark," and in (aa) even the diquark breaks up to form a fast-forward-moving quark. Such a diquark breakup was first proposed in Ref. 12. In Fig. 4 we show some examples for three-color-exchange contributions. For three or more collisions there would be in principle the possibility to "remove" three quarks from the projectile (target), thus leaving a fast-forward- (backward-) moving flavor white object (glueball)? We do not allow this possibility; we require a minimum number $N_s=1$ of surviving valence quarks; $N_s=2$ would prohibit diquark breakup; this is the usual assumption in dual parton models.[5–7] In the code VENUS N_s is a parameter; all results in this paper refer to $N_s=1$. Many global quantities such as multiplicity and transverse-energy distributions are only very weakly affected by the choice of N_s.

A new feature occurs in ultrarelativistic nucleon-nucleus collisions compared to N-N collisions. Since ultrarelativistic means by definition that the hadronization

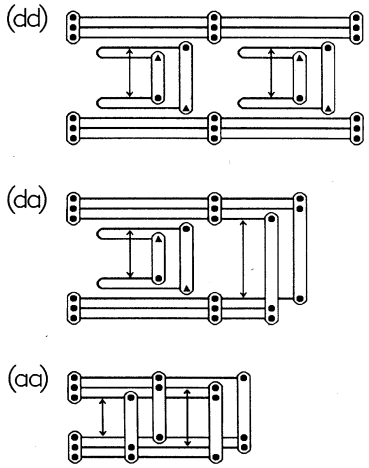

FIG. 3. Examples of two-color-exchange diagrams.

time for the projectile is larger than the nuclear size, it happens that a leading diquark or even a leading quark—produced in an earlier collisions—interacts with a target nucleon. Yet, the above definition of an N-N collision can be as well applied to such collisions between wounded nucleons: the interaction is realized by color exchange between quarks, which rearranges singlet structures to produce strings. The following restriction applies: we only consider quarks to participate in the color exchange which have not been struck in an earlier collisions. So for every single collision in a sequence of ν collisions of a projectile nucleon with target nucleons, we have the four basic one-color-exchange contributions $\sigma_1^a(\mu)$, $\sigma_1^b(\mu)$, $\sigma_1^c(\mu)$, $\sigma_1^d(\mu)$ as in Figs. 2(a)–2(d) ($1\leq\mu\leq\nu$ indicates that target nucleon μ is involved) and correspondingly higher-order contributions $\sigma_1^{m_1}(\mu)\sigma_1^{m_2}(\mu)\cdots\sigma_1^{m_i}(\mu)$. The whole contribution is [see Eqs. (3.1) and (3.3)]

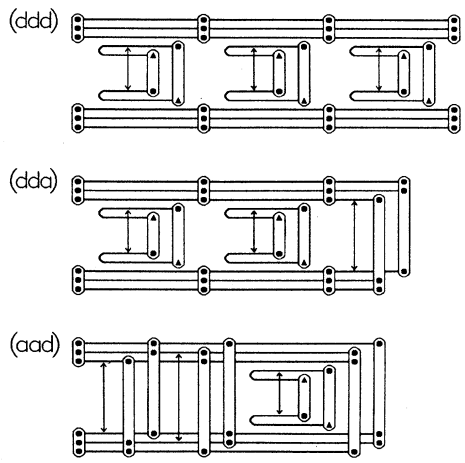

FIG. 4. Examples of three-color-exchange diagrams.

$$\prod_{\mu=1}^{\nu}\left[\sum_i w_i\sigma_i(\mu)\right]=\prod_{\mu=1}^{\nu}\left[\sum_i w_i\sum_{m_1\in M}\cdots\sum_{m_i\in M}\prod_{j=1}^{i}P(\sigma_1^{m_j})\prod_{j=1}^{i}\sigma_1^{m_j}(\mu)\right], \tag{3.4}$$

w_i being the probability for i color exchanges in an N-N collision and $M\equiv\{a,b,c,d\}$. In Fig. 5 we show as an example for $\nu=2$ the contribution $\sigma_1^a(1)\sigma_1^d(1)\sigma_1^a(2)$ and as an example for $\nu=3$ the term $\sigma_1^b(1)\sigma_1^a(2)\sigma_1^d(3)$. The entire nucleon-nucleus collision can be written as [with $P_A(\nu)$ being the probability to perform ν collisions]

$$\begin{aligned}\sigma_{pA}&=\sum_\nu P_A(\nu)\prod_{\mu=1}^{\nu}\left[\sum_i w_i\sum_{m_1\in M}\cdots\sum_{m_i\in M}\prod_{j=1}^{i}P(\sigma_1^{m_j})\prod_{j=1}^{i}\sigma_1^{m_i}(\mu)\right]\\&=\sum_\nu\sum_{i_1\cdots i_\nu}\sum_{m_1^1\in M}\cdots\sum_{m_{i_1}^1\in M}\cdots\sum_{m_1^\nu\in M}\cdots\sum_{m_{i_\nu}^\nu\in M}P_A(\nu)\prod_{\mu=1}^{\nu}w_{i_\mu}\left[\prod_{\mu=1}^{\nu}\prod_{j=1}^{i_\mu}P(\sigma_1^{m_j^\mu})\right]\left[\prod_{\mu=1}^{\nu}\prod_{j=1}^{i_\mu}\sigma_1^{m_j^\mu}(\mu)\right].\end{aligned} \tag{3.5}$$

How do we calculate string properties for a given contribution $\prod_i\sigma_1^{m_i}(\mu_i)$? The strings consist of the following ingredients: antiquarks with momentum fractions $\bar{x}_i(\mu)$ ($0\leq\mu\leq\nu$ referring to the nucleon), participating quarks with momentum fractions $x_i(\mu)$, and spectator partons (diquarks or quarks) with momentum fractions $z(\mu)$. Participants and spectators are meant regarding color exchange. Since spectators are thought to be dressed containing gluons and q-$\bar{q}$ pairs, we determine only momentum fractions of participating quarks and of antiquarks according to measured structure functions, the spectator gets what is left. So the momentum distribution of the relevant partons of nucleon μ is [with $x_i\equiv x_i(\mu)$, $\bar{x}_i=\bar{x}_i(\mu)$, $z=z(\mu)$]

$$f(\cdots x_i\cdots\bar{x}_j\cdots z)=\prod_i q_i(x_i)\prod_j\bar{q}_j(\bar{x}_j)\delta\left[1-\sum_i x_i-\sum_j\bar{x}_j-z\right]\theta(z). \tag{3.6}$$

Not knowing multiquark structure function, we make in Eq. (3.6) a simple factorization ansatz; the factor $\theta(z)$ reflects the fact that we do not allow to "remove" more momentum from the nucleon than available.

We are talking about momentum fractions, but we did not specify so far which kind of momentum we mean. The possibilities are the longitudinal momentum $p_\parallel$, the energy p_0, or the light-cone variable $p_+=p_\parallel+p_0$, all of them being equal (concerning fractions) for $p\to\infty$. In order to make a choice let us first evaluate the mass of a string in terms of the parton momenta $p(1)=(p_0(1),\mathbf{p}_t(1),p_\parallel(1))$ and $p(2)=(p_0(2),\mathbf{p}_t(2),p_\parallel(2))$. The string mass is

$$\begin{aligned}m^2=&[p_0(1)+p_0(2)]^2-[\mathbf{p}_t(1)+\mathbf{p}_t(2)]^2\\&-[p_\parallel(1)+p_\parallel(2)]^2.\end{aligned} \tag{3.7}$$

For vanishing longitudinal momenta we find

$$m^2=2|p_t(1)||p_t(2)|(1-\cos\alpha), \tag{3.8}$$

α being the angle between $\mathbf{p}_t(1)$ and $\mathbf{p}_t(2)$. The transverse momentum p_t being of the order (nucleon ra-

dius)$^{-1} \approx 0.4$ GeV, we find m to be of the order $(2 \times 0.4^2$ GeV$^2)^{1/2} \approx 0.6$ GeV which is considerably larger than the pion mass. This is very important, as we will see in the following. According to Duke and Owens[13] the quark structure functions are parametrized as (see also Ref. 14 for the parameters)

$$xq_i(x) = Ax^a(1-x)^b(1+\alpha x) , \tag{3.9}$$

with $a = 0$ for sea quarks. So some cutoff is necessary to handle the x^{-1} divergence for $x \to 0$. A natural cutoff is the requirement that the string mass has to be larger than the pion mass for q-$\bar{q}$ strings (or larger than the proton mass for qq-q strings). Since, as discussed above, the string mass due to relative motion in transverse direction is already larger than the pion mass, such a string-mass cutoff could not remove the x^{-1} divergence—if x is the longitudinal-momentum fraction. Consequently we have to use a variable, which includes p_t, the energy $p_0 = (p_\parallel^2 + p_t^2)^{1/2}$ or the light-cone variable $p_+ = p_0 + p_\parallel = (p_\parallel^2 + p_t^2)^{1/2} + p_\parallel$. It amounts to a kind of parameter to have the choice between p_0 and p_+. We prefer p_0 and all results in this paper are obtained in this way.

Independent of which momentum (p_0 or p_+) the fraction x refers to, we use, assuming cylindrical symmetry, as a second variable the absolute value of the transverse momentum $p_t = (p_x^2 + p_y^2)^{1/2}$. In general we generate p_t independent of x according to either an exponential distribution

$$f_1(p_t) \sim p_t \exp\left[-\frac{2}{\langle p_t \rangle} p_t\right] , \tag{3.10}$$

or according to a Gaussian distribution

$$f_2(p_t) \sim p_t \exp\left[-\frac{\pi}{4\langle p_t \rangle^2} p_t^2\right] , \tag{3.11}$$

with a parameter $\langle p_t \rangle$ of the order

$$\langle p_t \rangle \approx R^{-1} , \tag{3.12}$$

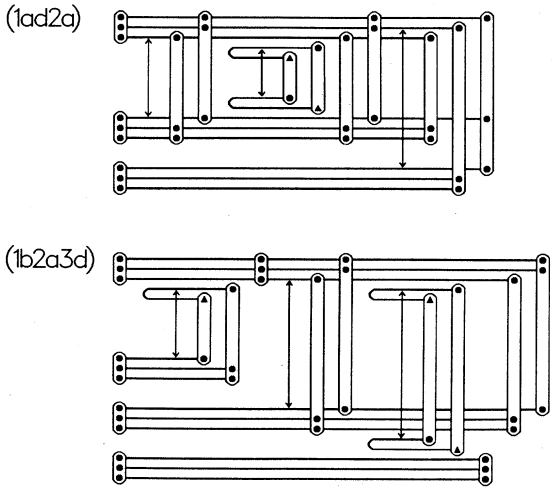

FIG. 5. Example for nucleon-nucleus interaction with two and three participating target nucleons.

R being the size of a nucleon. For all results obtained in this paper we use the exponential distribution f_1 with $\langle p_t \rangle = 0.400$ GeV. The variables x and p_t are, of course, not entirely independent since p_t has to be smaller than the energy xE_0.

Using the above prescription to determine string properties, we get, for example, a distribution of string rapidities

$$y = \tfrac{1}{2} \ln \frac{p_0(1) + p_0(2) + p_\parallel(1) + p_\parallel(2)}{p_0(1) + p_0(2) - p_\parallel(1) - p_\parallel(2)} \tag{3.13}$$

as shown in Fig. 6. In order to explain the results we give the asymptotic ($p \to \infty$) limit of Eq. (3.13) for finite x

$$y = \tfrac{1}{2} \ln \frac{x(1)}{x(2)} . \tag{3.14}$$

The value for x is qualitatively different for participating partons and spectators. Participants have small x according to the structure functions, which are peaked at small x, whereas spectators, as long as not too many participants contribute, carry a large momentum fraction. Therefore qq-q strings have a preferred direction. If the spectator is from the projectile ("projectilelike" qq-q string) they move forward ($y > 0$); if the spectator is from the target ("targetlike" q-q strings), they move backward ($y < 0$). Since for N-N collisions ($\nu = 1$, left Fig. 6) we have one projectilelike and one targetlike string, we observe two maxima of equal height around $y = \pm 1$. For $\nu = 3$ we still observe two maxima, also around $y = \pm 1$, yet the left ($y < 0$) peak is approximately three times as high as the right ($y > 0$) peak, because we have three targetlike qq-q strings versus only one projectilelike qq-q string. In general, we have for ν collisions ν targetlike and one projectilelike string, just reflecting baryon-number conservation. Since for q-$\bar{q}$ strings $x(1)$ and $x(2)$ are generated according to the same distribution $q(x)$ with a maximum at a small value of $x = x_0$, the rapidity distribution peaks at $y = 0$, yet showing large fluctua-

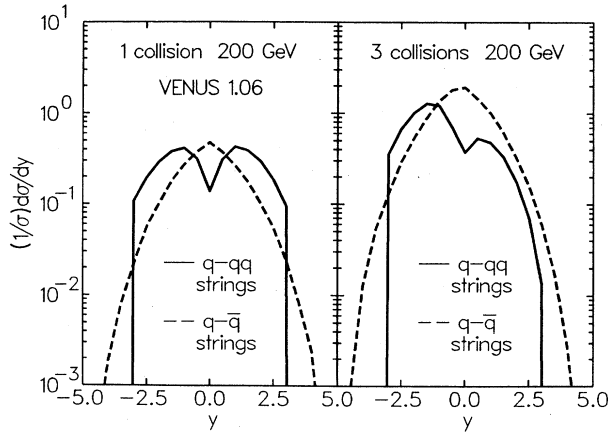

FIG. 6. Distribution of string rapidities for one and three collisions. The solid curves consider diquark-quark (qq-q) strings; the dashed curves consider quark-antiquark (q-$\bar{q}$) strings. The qq-q strings can be clearly separated into backward- (targetlike) and forward- (projectilelike) moving strings.

tions. In order to understand the different large-x behavior of qq-q and q-$\bar{q}$ strings, we use another way to express the rapidity in the ultrarelativistic limit (for $y>0$):

$$y=\ln\frac{2x(1)P_0}{\mu_t} , \tag{3.15}$$

$\mu_t=(p_0^2-p_\parallel^2)^{1/2}$ being the transverse mass of the string with $p_0=p_0(1)+p_0(2)$ and $p_\parallel=p_\parallel(1)+p_\parallel(2)$, and with $x(1)=p_0(1)/P_0$, where P_0 is the nucleon momentum. Since the mass of a qq-q string has to be larger than the nucleon mass m_N and $x(1)\leq 1$,we find, as an upper limit,

$$y_{qq\text{-}q}\leq\ln\frac{2P_0}{m_N}=y_N , \tag{3.16}$$

y_N being the rapidity of the incident nucleon (for 200 GeV, $y_N=3$). This sharp cutoff can be clearly seen in the rapidity distributions for qq-q strings in Fig. 6. For q-$\bar{q}$ strings the situation is different, since the string mass is not limited by the nucleon mass, but by the much smaller pion mass m_π—so we observe q-$\bar{q}$ strings with rapidities larger than y_N.

IV. STRING FRAGMENTATION

In this section we discuss particle production from a color string. We are, of course, interested in strings produced in hadronic collisions, as discussed above. Yet the following considerations are more general: the fragmentation model (with the same parameters) is also applied to describe particle production of strings from e^+e^- annihilation and deep-inelastic lepton nucleon scattering. So, we have the opportunity to test and fix the fragmentation procedure before applying it to hadronic collisions.

A string is defined by the flavor of the two partons that generate the string and by the parton momenta

$$p(1)=(p_0(1),\mathbf{p}_t(1),p_\parallel(1))$$

and

$$p(2)=(p_0(2),\mathbf{p}_t(2),p_\parallel(2)) ,$$

the latter ones defining string momenta

$$p=(p_0,\mathbf{p}_t,p_\parallel)\equiv p(1)+p(2) .$$

We first perform a Lorentz boost for the parton momenta $p(i)$ into the string c.m. system

$$\begin{aligned} p_0'(i)&=\beta_0 p_0(i)+\sum_{l=1}^{3}\beta_l p_l(i) ,\\ p_k'(i)&=\beta_k p_0(i)+p_k(i)\\ &\quad+\frac{\beta_k}{1+\beta_0}\sum_{l=1}^{3}\beta_l p_l(i) , \end{aligned} \tag{4.1}$$

with

$$\beta_\mu=\frac{p_\mu}{(p_0^2-p_1^2-p_2^2-p_3^2)^{1/2}},\quad \mu=0,1,2,3 \tag{4.2}$$

[we identify $\mathbf{p}_t=(p_1,p_2)$ and $p_\parallel=p_3$]. Two Euler angles

$$\begin{aligned} \cos\alpha&=\frac{p_3'(1)}{\{[p_2'(1)^2+p_3'(1)]\}^{1/2}} ,\\ \cos\beta&=\frac{\{[p_2'(1)^2+p_3'(1)^2]\}^{1/2}}{\{[p_1'(1)^2+p_2'(1)^2+p_3'(1)^2]\}^{1/2}} , \end{aligned} \tag{4.3}$$

define the tilt of the string relative to the three-axis. A rotation

$$\begin{bmatrix} p_1''(i)\\ p_2''(i)\\ p_3''(i)\end{bmatrix}=\hat{R}\begin{bmatrix} p_1'(i)\\ p_2'(i)\\ p_3'(i)\end{bmatrix} \tag{4.4}$$

with the transformation matrix

$$\hat{R}=\begin{bmatrix} \cos\beta & -\sin\alpha\sin\beta & -\cos\alpha\sin\beta\\ 0 & \cos\alpha & -\sin\alpha\\ \sin\beta & \sin\alpha\cos\beta & \cos\alpha\cos\beta\end{bmatrix} \tag{4.5}$$

provides a purely longitudinal string, all transverse momenta of the partons being zero. The inverse matrix (for the reverse transformation later) is

$$\hat{R}^{-1}=\begin{bmatrix} \cos\beta & 0 & \sin\beta\\ -\sin\beta\sin\alpha & \cos\alpha & \cos\beta\sin\alpha\\ -\sin\beta\cos\alpha & -\sin\alpha & \cos\beta\cos\alpha\end{bmatrix} . \tag{4.6}$$

After Lorentz boost and rotation a string is now well prepared to be processed by a string fragmentation procedure. Different types of models provided a phenomenological description of string fragmentation: (i) the Field-Feynman model[15] where the two partons fragment independently in an iterative manner, (ii) the Lund model[16] where resonance production is realized through breaking the string in pieces, (iii) parton-shower models[17] where ordered gluon radiation is the source of particle production. We use a generalized version of the Field-Feynman model (FFM), as described in the following.

In the FFM the two partons, which define the string, fragment essentially independently of each other. For each of the partons a fragmentation cascade is defined by elementary vertices; a parton (q or $\bar{q}$ or qq or $\overline{qq}$) produces a primary hadron, leaving a new parton with reduced momentum. Figure 7 shows the vertices we take into account: 7(a) a quark producing a meson, leaving a quark; 7(b) a quark producing a baryon, leaving an antidiquark; 7(c) a diquark producing a meson, leaving a diquark; and 7(d) a diquark producing a baryon, leaving an antiquark. The vertices for antiquark and antidiquark production are obtained by exchanging quarks and antiquarks.

The relative weights of baryon and meson production in quark jets ($P_q^b,1-P_q^b$) and in diquark jets ($P_{qq}^b,1-P_{qq}^b$) provide two free parameters. A further parameter is the probability P_s to create $s\bar{s}$ pairs in competition to $u\bar{u}$ and $d\bar{d}$ production. The latter two are assumed to be equally probably produced

$$P_u=\frac{1-P_s}{2},\quad P_d=\frac{1-P_s}{2} . \tag{4.7}$$

The momentum of a primary hadron relative to the momentum of the corresponding parton is generated ac-

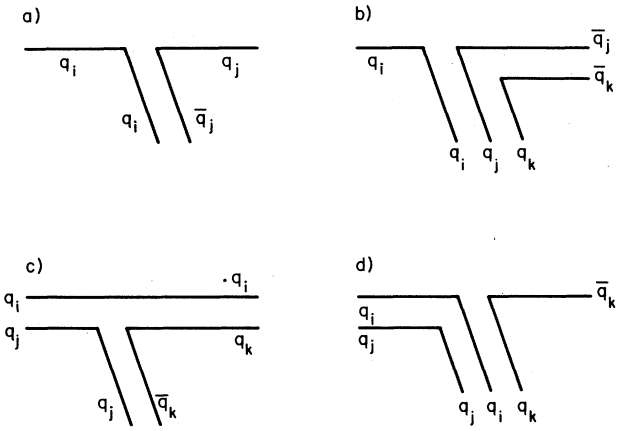

FIG. 7. The elementary fragmentation vertices for the fragmentation of quarks and diquarks.

cording to so-called splitting functions $f_q^m(x)$, $f_q^b(x)$, $f_{qq}^m(x)$, and $f_{qq}^b(x)$ for the four vertices of Fig. 7. The splitting functions are a crucial input of the model. They determine momentum distributions of produced particles, moreover, the multiplicities depend strongly on these functions. Therefore, one would like to have some theoretical basis to determine them, rather than having free parameters. Indeed, there exist QCD-inspired results for the asymptotic behavior of such elementary vertices as x approaches 1. The fragmentation behaves like $(1-x)^{2n-1}$, where n counts the number of spectators (counting rules[18]). We have $n=1$ for the vertices Figs. 7(a) and 7(d) and $n=2$ for the vertices Figs. 7(b) and 7(c), leading to a large-x behavior as $(1-x)^1$ and $(1-x)^3$, respectively. In order to account for the fact that one does *not* observe a rapidity plateau of baryons produced in deep-inelastic scattering[19] we add a factor x^α for the case of baryon production. We eventually use (up to normalization factors)

$$f_q^m(x)=(1-x),\quad f_q^b(x)=x^\alpha(1-x)^3\ ,$$
$$f_{qq}^m(x)=(1-x)^3,\quad f_{qq}^b(x)=x^\alpha(1-x)\ . \tag{4.8}$$

Again we have some freedom concerning the choice of the momentum variable: longitudinal momentum $p_\parallel$, energy p_0, or light-cone variable $p_+=p_\parallel+p_0$ (for large momentum they are equal). For all calculations presented we choose the energy p_0.

The transverse momentum p_t of quarks created during fragmentation is generated according to either an exponential distribution,

$$f_1(p_t)\sim p_t\exp\left[-\frac{2}{\langle p_t\rangle}p_t\right]\ , \tag{4.9}$$

or according to a Gaussian distribution,

$$f_2(p_t)\sim p_t\exp\left[-\frac{\pi}{4\langle p_t\rangle^2}p_t^2\right]\ , \tag{4.10}$$

the first option being used in this paper. Azimuthal symmetry is assumed. We use a mean transverse momentum $\langle p_t\rangle=0.400$ GeV. If the quark gets a momentum $\mathbf{p}_t$, the corresponding antiquark gets $-\mathbf{p}_t$.

The jet fragmentation cascade is terminated when the jet energy is too small to produce further particles. In order to achieve flavor conservation (and thus baryon-number conservation) we combine the two remaining partons of two corresponding jets to make a primary hadron. The last fragmentation step before the recombination is only performed if the sum of the masses of all produced particles, including the recombined one, is smaller than the string mass. In this way we obtain approximate energy conservation. We perform a correction procedure[20] in order to achieve exact energy conservation as follows. Since we work in the string c.m. system, the four-momentum of all produced particles i per string

$$\begin{pmatrix}p_0\\ \mathbf{p}_t\\ p_\parallel\end{pmatrix}=\begin{pmatrix}\sum_i p_0(i)\\ \sum_i \mathbf{p}_t(i)\\ \sum_i \mathbf{p}_\parallel(i)\end{pmatrix} \tag{4.11}$$

should be $(p_0,\mathbf{p}_t,p_\parallel)=(M,\mathbf{0},0)$, M being the string mass. Although momentum conservation is done correctly, $\mathbf{p}_t=0$ and $p_\parallel=0$, we find in general p_0 to deviate slightly from M. To fix that we rescale all particle momenta

$$\mathbf{p}_t(i)\to(1+\epsilon)\mathbf{p}_t(i)\ ,$$
$$p_\parallel(i)\to(1+\epsilon)\mathbf{p}_\parallel(i)\ ,$$
$$p_0(i)\to\{m(i)^2+(1+\epsilon)^2[p_t(i)^2+p_\parallel(i)^2]\}^{1/2}\ ,$$

such that the energy of the produced particles matches the string mass:

$$\sum_i\{m(i)^2+(1+\epsilon)^2[p_t(i)^2+p_\parallel(i)^2]\}^{1/2}=M\ . \tag{4.12}$$

The fragmentation procedure described above has been applied to describe particle production of strings from e^+e^- annihilation and deep-inelastic $\bar\nu p$, νp, μp scattering. For string masses between few and 12 GeV we can reproduce mean multiplicities, momentum, rapidity, and multiplicity distributions. Qualitative features are multiplicity $\langle n\rangle$ increases logarithmically with the energy as $\langle n\rangle=a+b\ln E$. Rapidity distributions shows a plateau-like behavior at $y_{\text{c.m.}}=0$. These features can be easily understood in a very simplified, therefore analytical solvable, version of the model, which we discuss in the following (see Ref. 15).

Let us consider the fragmentation of a fast-moving quark, taking into account only the dominant vertex Fig. 7(a)—meson production (baryon production from a quark is much less likely than meson production, so the model is somehow not unrealistic). If we do not care about the fact that the cascade has to stop at some point, we can write an integral equation for the momentum fraction distribution at produced particles:

$$D(x)=f(x)+\int_x^1 d\xi\, f(1-\xi)D\left[\frac{x}{\xi}\right]\frac{1}{\xi}\ , \tag{4.13}$$

$f(x)\equiv f_q^m(x)$ being the splitting function. The term $f(x)$

on the right-hand side of Eq. (4.13) represents mesons which are produced from the original quark in the first fragmentation step (first-rank meson). The integral in Eq. (4.13) counts higher-rank mesons: $f(1-\xi)d\xi$ is the probability to have, after the first fragmentation, a remainder quark with the momentum fraction ξ, the term $\xi^{-1}D(x/\xi)$ is the distribution of mesons produced from the remainder quark, renormalized by ξ^{-1}. The reasonable ansatz

$$f(x)=(n+1)(1-x)^n \tag{4.14}$$

allows an analytical solution of the integral Eq. (4.13):

$$D(x)=\frac{f(x)}{x} . \tag{4.15}$$

For small values of x ($x \ll 1$) we find

$$D(x)=\frac{n+1}{x} . \tag{4.16}$$

In the central region (small x) it is more convenient to use the rapidity rather than the momentum. Taking x to be the light-cone momentum fraction $x=p_+/p_+^{\text{init}}$ we find the relation

$$x=\frac{\mu}{p_+^{\text{init}}}e^y , \tag{4.17}$$

where $\mu=(m^2+p_t^2)^{1/2}$ is the transverse mass of the pion. With $dx/dy=x$ [from (4.17)] we conclude from Eq. (4.16) for the rapidity density in the central region

$$D(y)=n+1 , \tag{4.18}$$

implying that the height of the rapidity distribution stays constant with energy; only the width increases (logarithmically with energy), consequently leading to an energy dependence of the mean multiplicity as

$$\langle n \rangle = a + b \ln E . \tag{4.19}$$

These important features, rapidity plateau and logarithmic increase of $\langle n \rangle$ with energy, remain approximately true also for the realistic model described earlier (taking into account all vertices of Fig. 7).

V. RESULTS

In this section we want to study properties of particle production according to the string model for nucleon-nucleus collision as discussed in Secs. II, III, and IV. A comparison with data will be left to the next section. In particular, we want to compare the two reactions: (a) a proton hitting exactly one target proton and (b) a proton hitting exactly three target nucleons—two neutrons and one proton. We discussed earlier (in Fig. 6) the distribution of string rapidities. In Fig. 8 we display the rapidity distribution of produced negative particles (mostly π^-). By comparing the solid and the dashed lines we realize that for one collision particle production is mostly due to qq-q strings, whereas q-$\bar{q}$ strings (from diffractive processes and from higher-order color-exchange processes) play a minor role. For three collisions the q-$\bar{q}$ strings participate more strongly due to the fact that by definition no more than two quarks can be removed from the projectile, so for $\nu=3$ (even without higher-order terms) at least one q-$\bar{q}$ pair is involved. In Fig. 6 we showed that qq-q strings can be subdivided into forward- and backward-moving strings (projectilelike and targetlike). Therefore, we shown in Fig. 9 how qq-q contributions (the dashed curve in Fig. 8) can be subdivided into contributions from forward- and backward-moving qq-q strings. We realize that for three collisions the backward peak is approximately three times as high as the forward peak—in accordance with three targetlike strings compared to one projectilelike one. Not so obvious but nevertheless remarkable is the difference concerning the mean values $\langle y \rangle$ for backward and forward peak for one and three

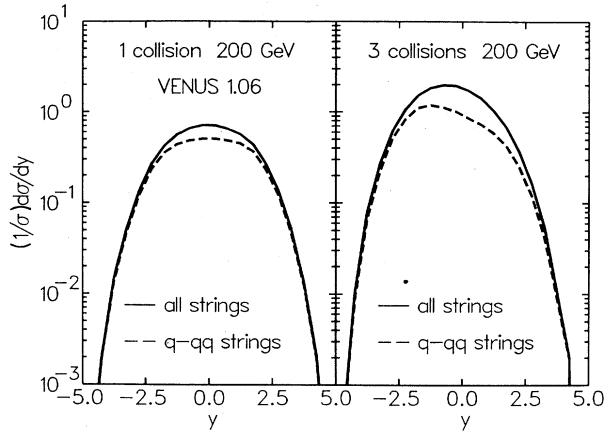

FIG. 8. Rapidity distribution of negative particles for one and three collisions. The solid curves represent the full distributions; the dashed curves only count for particles from qq-q strings.

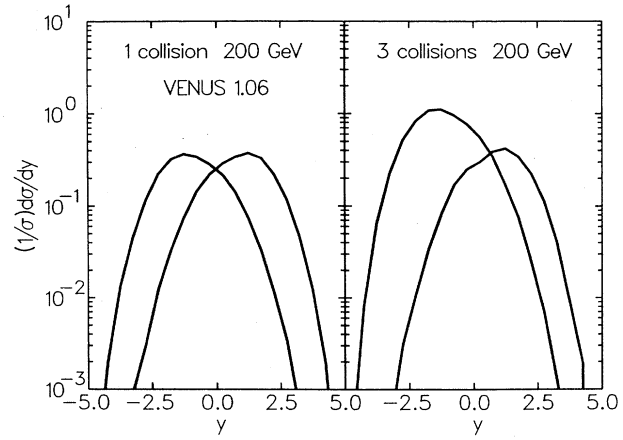

FIG. 9. Separation of rapidity distributions of particles from qq-q strings (dashed curves in Fig. 8) into contributions of particles from backward- and forward-moving strings. The backward peak for three-collision is approximately three times as high as the forward peak, corresponding to three times as many backward strings as forward strings.

collisions. We obtain

$$\langle y\rangle^1_{\text{backw}}=-0.92,\quad \langle y\rangle^1_{\text{forw}}=0.92\ ,$$
$$\langle y\rangle^3_{\text{backw}}=-1.14,\quad \langle y\rangle^3_{\text{forw}}=0.87\ . \tag{5.1}$$

Whereas the forward values are fairly close, we observe a substantial backward shift of the backward mean value for three collisions compared to one collision (see Ref. 21). This is partly due to the fact that for three collisions relatively more qq-q_{sea} strings compared to qq-q_{val} strings contribute than for one collision, and $\langle y\rangle_{\text{forw}}$ or $|\langle y\rangle_{\text{backw}}|$ is larger for qq-q_{sea} than for qq-q_{val} strings. The latter result is more or less obvious, since, as seen in Fig. 10, rapidity distributions of particles from qq-q_{val} strings are broader than distributions from qq-q_{sea} strings—yet on the quark side, since a valence quark has usually more momentum than a sea quark. On the diquark side, of course, both distributions look the same. For a relativistic string, the one end would not care what the other end looks like. This relativistic effect looks at first glance contradictory since we know that string rapidity and mass depends on both quark momentum and diquark momentum:

$$y_{\text{str}}=\tfrac{1}{2}\ln\frac{x(qq)}{x(q)}\ , \tag{5.2}$$

$$m_{\text{str}}=[s_{NN}x(qq)x(q)]^{1/2} \tag{5.3}$$

(we consider the ultrarelativistic limit). The rapidity of a particle (in forward direction, i.e., on the qq side), in the string c.m., is

$$y'_{\text{ptl}}=\ln\frac{\xi m_{\text{str}}}{\mu}=\tfrac{1}{2}\ln\frac{\xi^2}{\mu^2}sx(qq)x(q)\ , \tag{5.4}$$

ξ being a number between 0 and 1 and μ being the transverse mass of the particle. In the N-N reference system

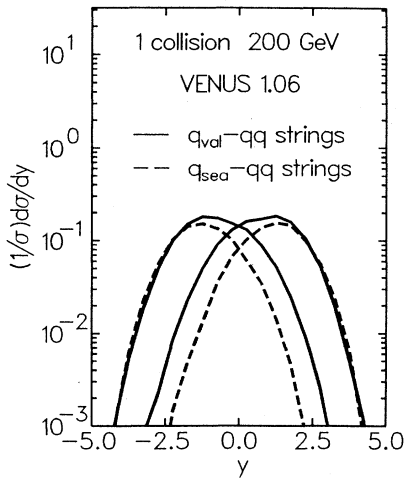

FIG. 10. Separation of the forward and backward qq-q string contributions in qq-q_{val} and qq-q_{sea} contributions. For large $|y|$, both agree, which means that the diquark side does not care about the parton at the other end of the string.

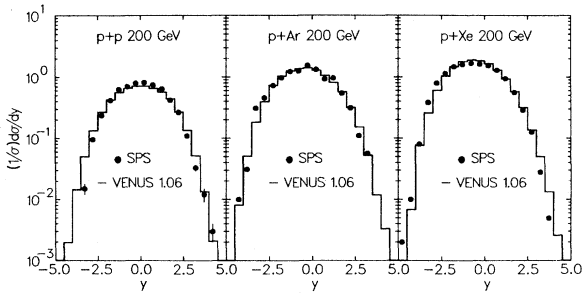

FIG. 11. Rapidity distribution of negative particles compared to data of De Marzo *et al.* (Ref. 22).

we find, with (5.2) and (5.4),

$$y_{\text{ptl}}=y'_{\text{ptl}}+y_{\text{str}}$$
$$=\frac{1}{2}\left[\ln\frac{\xi^2}{\mu^2}sx(qq)x(q)+\ln\frac{x(qq)}{x(q)}\right]$$
$$=\tfrac{1}{2}\ln\frac{\xi^2}{\mu^2}sx(qq)^2=\ln\frac{\xi\sqrt{s}\,x(qq)}{\mu}\ .$$

So the particle rapidity in fact does not depend on $x(q)$, the momentum of the proton on the other side. These considerations justify models for particle production in the projectile fragmentation region, which do not care about the backward parton.[11,12,14]

VI. COMPARISON WITH p-p, p-Ar, AND p-XE DATA

We are now going to compare results of our multistring model, carried out with the computer code VENUS 1.06, with data[22,23] for p-p, p-Ar, and p-Xe scattering at 200 GeV incident energy. Since our model does not include intranuclear cascading of secondaries, we will in particular care about how much room is left for particle production due to this effect. In Fig. 11 we see that the Monte Carlo results (histograms) reproduce the increase of particle production at backward rapidities for increasing target size, due to the increasing number of targetlike qq-q strings, as discussed earlier. At forward rapidities, data as well as calculated results are more or less the

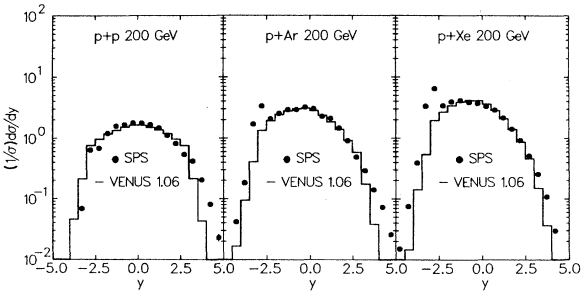

FIG. 12. Rapidity distribution of charged particles compared to data of De Marzo *et al.* (Ref. 22). Contrary to the model, the data show a spike at $y_{\text{lab}}\approx 0$, probably due to protons from the target remnant.

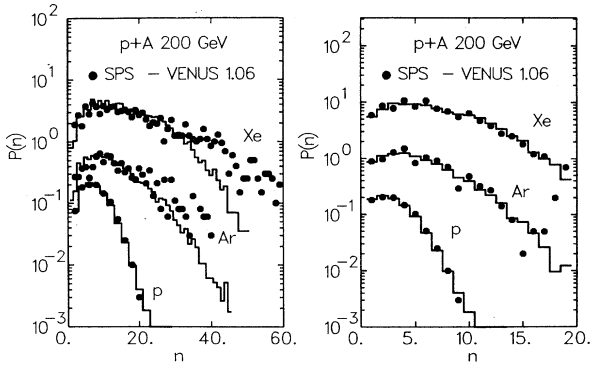

FIG. 13. Multiplicity distribution of charged (left) and negative (right) particles for p-p, p-Ar, and p-Xe scattering at 200 GeV. The data are from Ref. 22.

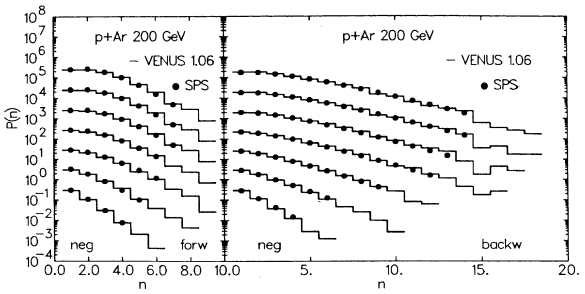

FIG. 15. Multiplicity distribution of negative particles in a p-Ar collision at 200 GeV in forward intervals $0<y<y_i$ (left) and backward intervals $-y_i<y<0$ (right) with $y_i=3.5,3.0,\ldots,0.5$ (from top to bottom). The data are from Ref. 23.

same for p-p, p-Ar, and p-Xe—since we have in any case only one projectilelike string. It is remarkable that even in the target-fragmentation region $[y\approx(-2)-(-3)]$ the agreement is satisfactory—leaving not much room for negative particle production due to cascading. The situation is quite different concerning charged particles (including protons). As seen from Fig. 12, the data (dots) are well reproduced by VENUS calculations (histograms), except for peaks around $y_{\text{c.m.}}=-3$ ($\Longrightarrow y_{\text{lab}}=0$) for p-Ar and p-Xe. These peaks are certainly due to slow proton from the fragmentation of the spectator part of the target nucleus. Spectators are not considered in our calculations at all. The flatter tails of the data for $y\gtrsim 3$ compared to VENUS look like misidentification of protons. A too-small transverse mass results in a too-large rapidity. In Fig. 13 we display multiplicity distributions for charged (left) and negative (right) particles. Again for negative particles VENUS results and data agree remarkably well, whereas the theoretical distribution for charged particles in p-Ar and p-Xe are much too narrow. Again we can blame the missing spectator protons for this disagreement. More detailed information is obtained by presenting multiplicity distributions in limited rapidity intervals ($y_{\min}<y<y_{\max}$), where only particles with a rapidity between $y_{\min}$ and $y_{\max}$ are counted. In Ref. 23 multiplicity distributions are presented separately for backward rapidity intervals ($-y_i\le y\le 0$) and forward intervals ($0\le y\le y_i$) with $y_i=\{0.5,1.0,1.5,2.0,2.5,3.0,3.5\}$. It turned out that all distributions can be well parametrized by the two-parameter negative-binomial (NB) distribution

$$p(n;k,\bar{n})=\frac{k(k+1)\cdots(k+n-1)}{n!}\frac{\bar{n}^{\,n}k^{k}}{(\bar{n}+k)^{n+k}}\ , \tag{6.1}$$

so we compare VENUS results with NB fits to these data. As seen from Fig. 14 VENUS reproduces both charged- and negative-particle distributions for p-p quite well, although the theoretical curves are slightly too narrow corresponding to a slight underprediction of the rapidity density (see Figs. 11 and 12). In Figs. 15–18 we show p-Ar and p-Xe results. On the right-hand side we alway plot the distributions for backward-rapidity intervals ($-y_i<y<0$), on the left-hand side for the forward intervals ($0<y<y_i$) with $y_i=3.5,3.0,\ldots,0.5$ from the top to the bottom. We first observe that backward distributions are much broader than forward distributions, being related to the fact that rapidity densities $\sigma^{-1}d\sigma/dy$ are

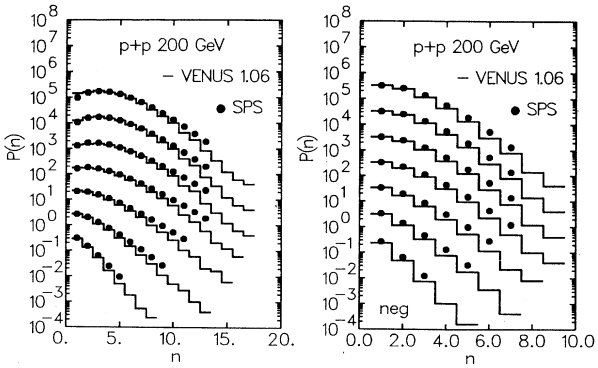

FIG. 14. Multiplicity distribution of charged (left) and negative (right) particles at limited rapidity intervals $0<y<y_i$ with $y_i=3.5,3.0,\ldots,0.5$ (from top to bottom) for a p-p collision at 200 GeV. The data are from Ref. 23.

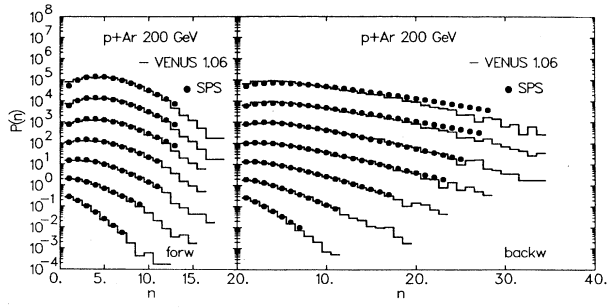

FIG. 16. Same as Fig. 15, but for charged particles.

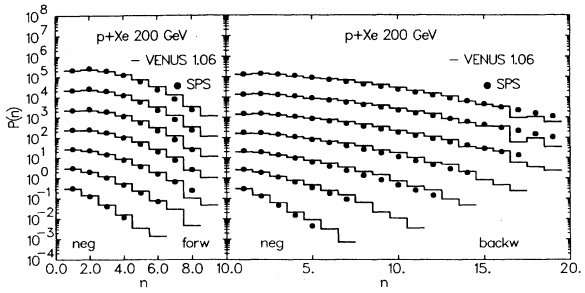

FIG. 17. Same as Fig. 15, but for p-Xe.

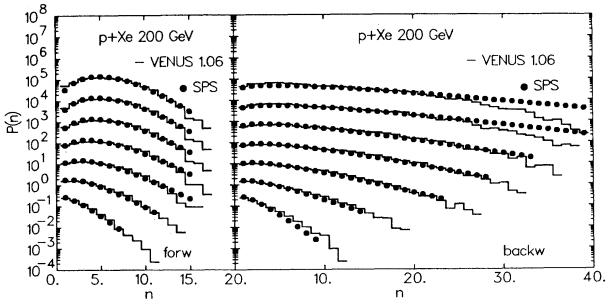

FIG. 18. Same as Fig. 17, but for charged particles.

peaked at negative rapidities (see Figs. 11 and 12), as discussed earlier (more targetlike than projectilelike strings contribute). For negative particles forward and backward distributions are nicely reproduced by VENUS. For charged-particle distributions only for the backward intervals $[-3.5,0]$ and $[-3.0,0]$ we observe a major disagreement. On the other hand, this includes just the rapidity $y \approx -3$ where we observed earlier an excess of charged particles compared to VENUS, probably due to spectator protons.

VII. CONCLUSIONS

We have demonstrated that the multistring model VENUS, a parameter-free extrapolation of a nucleon-nucleon model, is able to describe rapidity and detailed multiplicity distributions for p-p, p-Ar, and p-Xe collisions at 200 GeV reasonably well. Only some charged particles at $y_{\text{lab}}=0$ are missing, probably spectator protons. The effect of particle production due to cascading has to be carefully investigated; in fact we believe that p-nucleon data provide a much better and clearer test of such a concept that nucleus-nucleus data.

ACKNOWLEDGMENTS

I gratefully acknowledge discussions with R. Lonacre, T. Ludlam, S. Kahana, A. Matheson, F. Paige, A. Shor, and M. Tannenbaun. The code VENUS uses the subroutine DECAY as well as a decay table from F. Paige's code ISAJET. The submitted manuscript has been authored under Contract No. DE-AC02-76CH00016 with the U.S. Department of Energy. Die Arbeit wurde mit Unterstützung eines Stipendiums des Wissenschaftsausschuesses der NATO über den DAAD ermöglicht.

[1] *Quark Matter '86,* proceedings of the Fifth International Conference on Ultrarelativistic Nucleus-Nucleus Collisions, Asilomar, California, 1987, edited by L. Schroeder and M. Gyulassy [Nucl. Phys. **A461**, Nos. 1 and 2 (1987)].

[2] *Quarks Matter '87,* proceedings of the Sixth International Conference on Ultrarelativistic Nucleus-Nucleus Collisions, edited by H. Satz, H. J. Specht, and R. Stock [Z. Phys. C **38** (1988)].

[3] B. Anderson, G. Gustafson, and B. Nielsson-Almqvist, Nucl. Phys. **B281**, 289 (1987).

[4] M. Gyulassy, Report No. CERN-TH 4794/87 (unpublished).

[5] A. Capella and J. Tran Thanh Van, Z. Phys. C **10**, 249 (1981); A. Capella, T. A. Casado, C. Pajares, A. V. Ramello, and J. Tran Thanh Van, *ibid.* **33**, 541 (1987).

[6] J. Ranft and S. Ritter, Z. Phys. C **27**, 413 (1985); P. Aurenche, F. W. Bopp, and J. Ranft, *ibid.* **23**, 67 (1984).

[7] T. P. Pansart, in *Quark Matter '86* (Ref. 1).

[8] K. Werner, in *Quark Matter '87* (Ref. 2).

[9] K. Werner, in *Proceedings of the Third Conference on Intersections Between Particle and Nuclear Physics,* Rockport, Maine, 1988, edited by G. Bunce (AIP Conf. Proc. Vol. No. 176) (AIP, New York, 1988), p. 1053.

[10] R. J. Glauber and G. Matthiae, Nucl. Phys. **B21**, 135 (1970).

[11] K. Werner and M. Kutschera, Phys. Lett. B **183**, 385 (1987).

[12] K. Werner, J. Hüfner, M. Kutschera, and O. Nachtmann, Phys. Rev. Lett. **57**, 1684 (1986).

[13] D. W. Duke and J. F. Owens, Phys. Rev. D **30**, 49 (1984).

[14] K. Werner, J. Hüfner, M. Kutschera, and O. Nachtmann, Z. Phys. C **37**, 57 (1987).

[15] R. D. Field and R. P. Feynman, Nucl. Phys. **B136**, 1 (1978).

[16] B. Anderson, G. Gustafson, G. Ingelman, and T. Sjöstrand, Phys. Rep. **97**, 31 (1983).

[17] G. Marchesini and B. R. Webber, Nucl. Phys. **B238**, 1 (1984); B. R. Weber, *ibid.* **B238**, 492 (1984).

[18] J. F. Gunion, in *Proceedings of the 11th International Symposium on Multiparticle Dynamics,* Bruges, Belgium, 1980, edited by E. De Wolf and F. Yerbeure (University of Antwerp, Antwerp, Belgium, 1980), p. 767.

[19] European Muon Collaboration, M. Arneodo *et al.*, Z. Phys. C **31**, 1 (1986).

[20] F. E. Paige and S. S. Protopopescu, in *Physics of the Superconducting Super Collider, Snowmass, 1986,* proceedings of the Summer Study, Snowmass, Colorado, edited by R. Donaldson and J. Marx (Division of Particles and Fields of the APS, New York, 1987), pp. 320–325.

[21] A. Klar and J. Hüfner, Phys. Rev. D **31**, 491 (1985).

[22] C. De Marzo *et al.*, Phys. Rev. D **26**, 1019 (1982).

[23] F. Dengler *et al.*, Z. Phys. C **33**, 187 (1986).